Prediction of Speaker Performance at High Amplitudes

W. Klippel
Klippel GmbH
Germany

ABSTRACT
A new method is presented for the numerical simulation of the large signal performance of drivers and loudspeaker systems. The basis is an extended loudspeaker model considering the dominant nonlinear and thermal effects. The use of a two-tone excitation allows the response of fundamental, DC-component, harmonics, and intermodulation components to be measured as a function of frequency and amplitude. After measurement of the linear and nonlinear parameters, the electrical, mechanical, and acoustical state variables may be calculated by numerical integration. The relationship between large signal parameters and non-linear transfer behavior is discussed by modeling two drivers. The good agreement between simulated and measured responses shows the basic modeling, parameter identification, and numerical predictions are valid even at large amplitudes. The method presented reduces time-consuming measurements and provided essential information for quality assessment and diagnosis. The extended loudspeaker model also allows prediction of design changes on the large signal performance by changing the model parameters to reflect the driver design changes. The incorporation of nonlinear parameters into the loudspeaker model allows for optimization in both the small and large signal domains by model prediction.

Introduction

For many years linear models have been used for predicting and simulating the loudspeaker behavior [1-3]. Linear models assume a linear relationship between the input and output for any signal amplitude. However, a real speaker limits and distorts the output at higher amplitudes due to thermal and nonlinear mechanisms inherent in the driver, enclosure and radiation. Clearly, linear models fail at high amplitudes and are restricted to the small signal domain. However, assessing and improving the large signal performance becomes more and more an issue in loudspeaker design. Professional, multimedia, automotive and hi-fi applications require small, light-weight drivers manufactured at low cost generating the acoustical output at high efficiency and low distortion. New adequate tools are required for mastering the current challenges.

This paper starts with a summary of the current state of large signal modeling and parameter identification. Then alternative ways for assessing the vibration and transfer behavior at high amplitudes are discussed. Traditional and new measurement techniques applied to the real speaker will be compared addressing the question about a suitable excitation signal. Alternatively, a numerical technique will be presented to predict the transfer functions using the identified model. The agreement between measured and predicted responses will be investigated on two example drivers. The relationship between the driver parameters and the resulting transfer responses will be discussed in detail to understand complicated effects such as the dynamic generation of a DC-component which shift the coil out of the gap. After understanding the mechanisms in the particular driver conclusions for practical improvements can be derived.

Large Signal Modeling

At first we give a short overview on the large signal modeling [4-11] of electro-dynamical drivers mounted in enclosures which considers the dominant driver nonlinearities and a simple model for the thermal mechanisms.

State Variables

The state of a speaker operated at low frequencies where the wavelength is large in comparison to the geometrical dimension can be described by using the following quantities

$x(t)$	displacement of the voice coil,
$v(t)$	velocity of the voice coil,
$i(t)$	the electric input current,
$u(t)$	the driving voltage at loudspeaker terminals,
$p_{box}(t)$	sound pressure in enclosure (AC-part),
$q_P(t)$	volume velocity in port,
$p_{rear}(t)$	sound pressure in rear enclosure,
$p_{far}(t)$	sound pressure in the far field.

Lumped Parameter Model

The relationship between the state variables may be described by a lumped parameter model comprising a few number of elements characterized by parameter values. The number and kind of the lumped elements and the way how they are connected may be called the topology of our model. It is may be graphically represented as an electrical equivalent circuit as shown in Fig. 1. The speaker may be considered as a transducer coupling the electrical, mechanical and acoustical domain. In contrast to the traditional linear modeling some parameters are not constant but depend on instantaneous state variables.

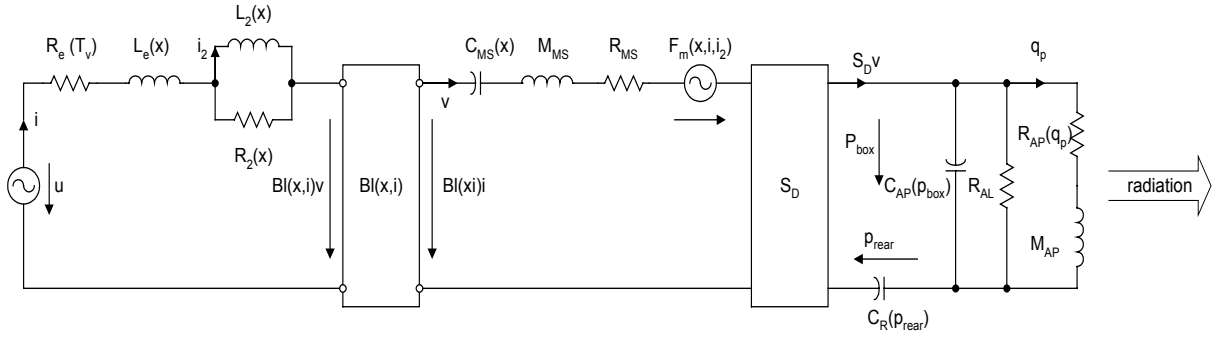

Fig. 1. Lumped parameter model of the driver mounted in enclosure

Electrical Driver Parameters

The electrical part comprises the following elements:

$R_e(T_V)$	DC resistance of voice coil,
$L_E(x)$	part of voice coil inductance which is independent on frequency,
$L_2(x)$	represents the para-inductance of the voice coil and
$R_2(x)$	the electric resistance due to additional losses caused by eddy currents.

Mechanical Driver Parameters

A transformer with the coupling factor

$$Bl(x,i) = Bl(x) + b_f(x)i \tag{1}$$

connects the electrical with the mechanical domain where

$Bl(x)$	is the effective instantaneous electrodynamic coupling factor (force factor of the motor) defined by the integral of the permanent magnetic flux density B over voice coil length l,
$b_f(x)$	is effective flux modulation factor caused by alternating magnetic field generated by the voice coil current.

The variation of the magnetic field energy versus voice coil displacement also generates a reluctance force $F_m(x,i,i_2)$ which can be approximated by

$$F_m(x,i,i_2) \approx -\frac{i(t)^2}{2}\frac{\partial L_E(x)}{\partial x} - \frac{i_2(t)^2}{2}\frac{\partial L_2(x)}{\partial x}. \tag{2}$$

The mechanical system is represented by the following elements

M_{MS}	mechanical mass of driver diaphragm assembly including voice-coil and air load,
R_{MS}	mechanical resistance of driver suspension losses,
$C_{MS}(x,t)$	mechanical compliance of driver suspension (the inverse of stiffness $K_{MS}(x,t)$.

Acoustical Parameters

The diaphragm represented by parameter

S_D effective projected surface area of driver diaphragm

combines the mechanical and acoustical domain.

The driver in an infinite baffle and mounted in different kinds of enclosures (band-pass, sealed, vented) may be modeled by using the following elements:

R_{AB} acoustic resistance of enclosure losses caused by internal energy absorption,

R_{AL} acoustic resistance of enclosure losses caused by leakage,

M_{AP} acoustic mass of port or vent including air load,

R_{AP} acoustic resistance of port or vent losses,

$C_{AB}(p_{box})$ acoustic compliance of air in enclosure,

$C_R(p_{rear})$ acoustic compliance of air in rear enclosure in band-pass systems,

V_R volume of air in rear enclosure in band-pass systems,

V_{AB} volume of air in enclosure.

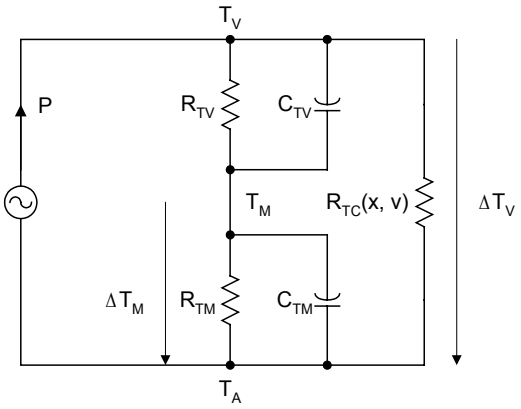

Fig. 2. Thermal model of the loudspeaker driver

Thermal Modeling

The heating of the voice coil is modeled by a thermal equivalent circuit as shown in Fig. 2. comprising the following elements and state variables:

R_{TV} thermal resistance of path from coil to magnet structure,

R_{TM} thermal resistance of magnet structure to ambient air,

$R_{TC}(x, v)$ thermal resistance due to air convection depending on the voice coil displacement and velocity,

C_{TV} thermal capacitance of voice coil and nearby surroundings,

C_{TM} thermal capacitance of magnet structure.

$P(t)$ real electric input power,

$T_V(t)$ temperature of the voice coil,

$T_M(t)$ temperature of the magnet structure,

$\Delta T_V(t) = T_V(t) - T_A$ increase of voice coil temperature,

$\Delta T_M(t) = T_M(t) - T_A$ increase of the temperature of magnet structure,

T_A temperature of the cold transducer (ambient temperature).

State Space Equation

We assume that all effects of the acoustical environment and the radiation impedance may be represented by the acoustical and mechanical parameters in Fig. 1 which are independent on the radiated sound pressure p_{far}.

Thus, the differential equation written in the general state space form is

$$\dot{z} = \mathbf{a}(z)\,z + \mathbf{b}(z)\,u \tag{3}$$

where u *is* the voltage at the terminals of the voltage driven loudspeaker, $\boldsymbol{z}(t)=[x_p,\ dx_p/dt,\ i,\ q_P,\ p_{box},\ i_2,\ p_R]^T$ is the state vector of the system, and the matrix **a** and the vector **b** comprise lumped parameters depending on the state vector $\boldsymbol{z}$. The graphical representation of the state space form in Fig. 3 reveals a feed-back structure where all the distorted signals in the state vector $\boldsymbol{z}$ react via the nonlinear parameters on the input of the system.

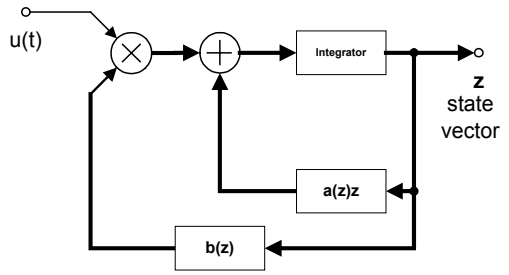

Fig. 3. State space model

Radiation

The sound pressure signal in the far field radiated from a closed and vented-box system may be approximated by

$$p_{far}(t,r) = \frac{d^2\left(C_{AB}(p_{box})p_{box}\right)}{dt^2}\frac{\rho}{2\pi r}e^{-s(r-x))/c} \tag{4}$$

with

ρ density of air,

c speed of sound,

r distance between diaphragm and listening position.

The exponential term represents phase modulation due to the Doppler effect depending on the instantaneous voice coil displacement x.

For a band-pass system the sound pressure signal in the far field is

$$p_{far}(t,r) = \frac{dq_p}{dt}\frac{\rho}{2\pi r}. \tag{5}$$

Identification of the Driver Model

The large signal model of the speaker comprises structural information, parameters and state variables. The first task of the model identification is to prove that the topology is adequate for the type of transducer and the principle of conversion used. The second task of the model identification is to specify the free parameters of the model for the particular unit. In the third step all of the state variables and the output signal may be predicted for any input signal using an adequate topology and optimal parameters.

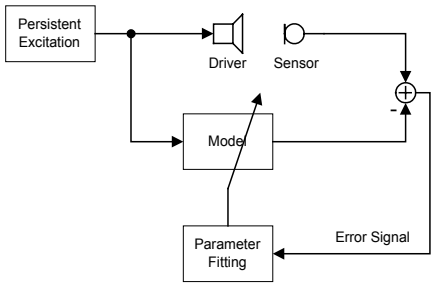

Fig. 4. Identification of the driver model

The identification of model is usually based on the measurement of one or more state variables as shown in Fig. 4. The speaker is persistently excited by a broad band signal and an electrical, mechanical or acoustical signal is measured. Monitoring the electric input current at the terminals and detection of the back EMF gives a signal proportional to the voice coil velocity and dispenses with an expensive sensor.
Connecting the model in parallel to the driver/sensor system the agreement between driver and model may be evaluated by an error signal which is the difference between measured and predicted output. The parameters may be adaptively adjusted to optimal estimates by reducing the amplitude of the error signal with a LMS-algorithm.
Implementing this approach in a digital system (DSP) we may perform system identification on-line for any audio input while operating the driver under normal working conditions [13 – 14]. An error signal of low amplitude proves that the model topology is adequate and optimal estimates on the parameters are found.

Assessing Transfer and Vibration Behavior

The behavior of the loudspeaker may also be described by the relationship between the input signal *u(t)* and the state variables or the output signal. Assuming a linear system the impulse response or the system function represented as amplitude and phase response gives us all information about this relationship. A weakly nonlinear system may be adequately modeled by the Volterra-series comprising higher-order system functions. Unfortunately, this approach fails in describing accurately the behavior of speakers at higher amplitudes because the feed-back structure shown in Fig. 3 does not correspond with the feed-forward structure of the Volterra-series where a linear, quadratic and other higher-order homogenous system are connected in series.
Alternatively, we may use a special excitation signal and investigate the effect in the output or state variables.
A two tone signal defined by

$$u(t) = U_1 \sin(2\pi f_1 \cdot t) + U_2 \sin(2\pi f_2 \cdot t) \qquad \textbf{(6)}$$

is an optimal excitation signal because the spectral components of the measured signal may be easily interpreted as fundamental, DC-component, harmonic, sub-harmonic, difference-tone and summed-tone intermodulation distortion as shown in Fig. 5.

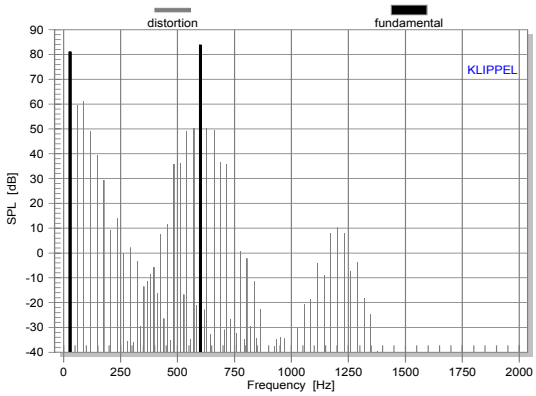

Fig. 5. Spectrum of sound pressure signal of a two-tone excitation signal (bold lines) and distortion components (thin lines)

The frequencies f_1 and f_2 and the amplitude U_1 and U_2 may be varied to perform frequency and amplitude sweeps. For the measurement of summed-tone or difference tone intermodulation components there are three modes of special interest:

- The frequency f_2 is held constant during frequency sweep of f_1. This mode allows to generate a very critical stimulus for most transducers. Selecting $f_2 < f_1$, f_2 may represent a bass tone producing large voice coil displacement and f_1 represents any audio component (voice) in the pass band of the transducer.
- The frequency ratio f_2/f_1 is held constant between both excitation tones. Selecting $f_2 > f_1$ and using a fractional ratio (e.g. 5.5) this mode avoids interferences between the harmonic and intermodulation distortion components.
- The distance f_2-f_1 between both excitation frequencies is constant during the frequency sweep of f_1. This mode produces difference intermodulation at the same frequency independent of f_1.

The driver variables in steady state condition are subject to a FFT analysis. Using frequencies f_1 and f_2 of the excitation tones at values consistent with the FFT length, additional windowing of the time signal can be omitted. This reveals the spectral components without any smearing effects.
The transfer behavior may be measured, predicted or simulated depending on the way how the state variables are provided.

Measurement

The measurement of the state variables and the output signal as illustrated in Fig. 6 is the most simple way for assessing the transfer behavior.

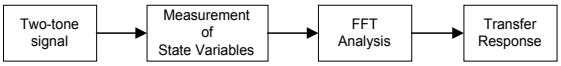

Fig. 6. Measurement of the transfer response

Measurements of electrical current and sound pressure can be accomplished with normal equipment. The measurement of the displacement requires a special sensor but an inexpensive laser based on triangulation becomes more and more an indispensable tool for driver development. For the measurement of the air velocity in the port a hot-wire anemometer is usually not available.

Prediction

Having an adequate model topology and valid parameters for the particular driver and enclosure we may predict the state variables z

for any input signal u(t) by integrating the state space equation starting at the initial conditions $z(t=0)$ as illustrated in Fig. 7.

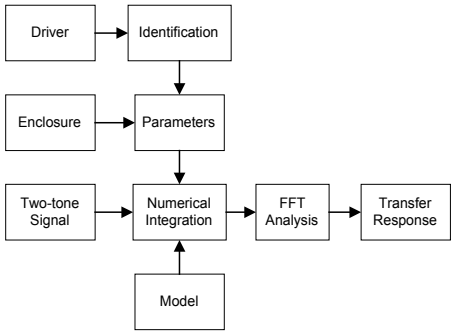

Fig. 7. Prediction of the Transfer Response

The numerical integration may be accomplished by the classical explicit Runge-Kutta method or more sophisticated solvers with step size control giving higher precision. For certain combinations of the driver parameters the differential equation behaves stiff and special solver techniques are required.

Comparing the predicted response with the response based on easy to do electrical current or sound pressure measurements is a simple test to prove that the modeling is valid and the parameters are reliable. Then the measurements of other variables requiring special sensors may be replaced by numerical predictions.

Simulation

Whereas the prediction uses the parameters of a real loudspeaker system we may also simulate the behavior of a virtual loudspeaker before the first prototype has been finished. The parameters may be produced by FEM-calculations or by simply modifying the parameters of an existing speaker to assess design choices as illustrated in Fig. 8.

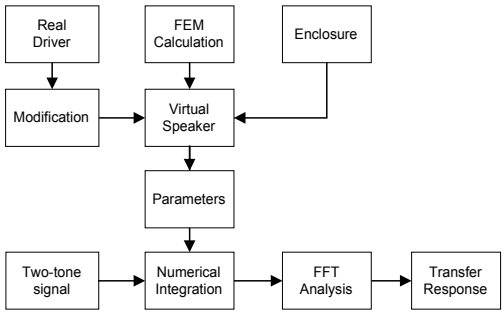

Fig. 8. Simulation of the transfer response

To investigate the effect of each nonlinearity separately and to find the dominant source of distortion the following nonlinearities might be switched on and off during simulation:

- motor nonlinearity due to $Bl(x)$
- mechanical suspension nonlinearity due to $C_{ms}(x)$
- inductance nonlinearity due to $L_e(x)$
- para-inductance nonlinearity due to $L_2(x)$
- losses from eddy currents due to $R_2(x)$
- reluctance force (electromagnetic drive)
- adiabatic compression in enclosure $C_{AB}(P_{box})$
- adiabatic compression of rear enclosure $C_R(P_{rear})$
- radiation distortion (Doppler effect)

Practical Application

Numerical prediction and simulation of the transfer response not only confirm the results of direct measurements but also provide additional information which are crucial for the assessment of loudspeaker systems. These tools will be applied to two drivers (Driver A and B) used as case studies in the following paper. The drivers differ in design, parameters and behavior significantly. Both drivers are intended for high-quality applications.

Parameters	Driver A	Driver B	Unit
f_s	30.5	28.9	Hz
$Bl(x=0)$	7.43	4.99	N/A
$C_{MS}(x=0)$	1.28	3.69	mm/N
$Le(x=0)$	0.47	0.32	mH
L_2	0.32	0.16	mH
M_{MS}	21.1	8.21	g
Q_{MS}	2.87	7.99	
R_2	2.18	1.37	Ohm
R_E	3.54	5.99	Ohm
R_{TM}	0.62	1.07	K/W
R_{TV}	2.153	5.53	K/W
C_{TV}	11.53	3.79	J/K

Table 1. Thermal and nonlinear parameters at the rest position

Driver A

Driver A is an 8 inch woofer with a relatively high force factor as shown in Table 1. This corresponds with a short voice coil overhang causing an early decay of the Bl-product at small displacement as shown in Fig. 9.

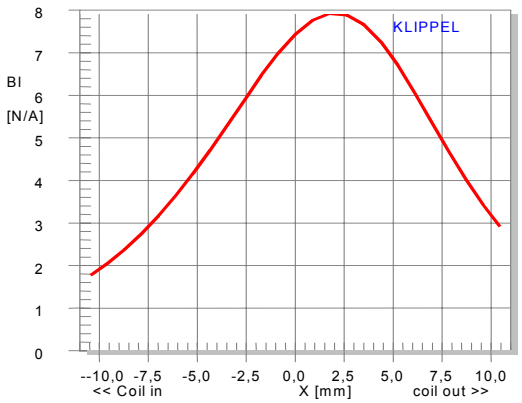

Fig. 9. Force factor $Bl(x)$ versus displacement x of Driver A

The voice coil height corresponds approximately with the peak to peak displacement of 14 mm where the instantaneous force factor value decays to 50% of the maximal value. The rest position of the coil is not in the Bl-maximum producing a significant asymmetry in the curve.

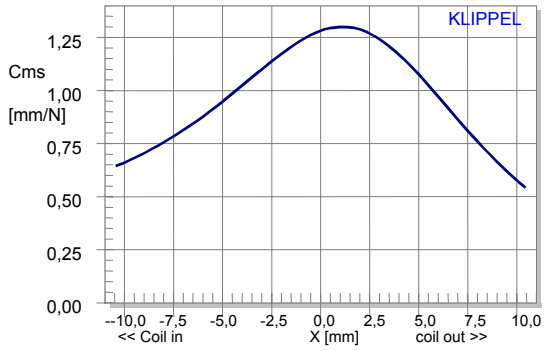

Fig. 10. Compliance $C_{ms}(x)$ versus displacement x of Driver A

Whereas the capability of the motor is almost exhausted at x = - 9 mm the compliance of the suspension decreases only down to 44% as shown in Fig. 10. Most suspensions handle a variation of $C_{ms}(x)$ down to 20 % without causing any damage. The maximum of the compliance is not at the rest position but for higher positive displacement the compliance decreases faster than for negative displacement giving almost the same compliance at x = +- 7 mm. Thus, the symmetry of the suspension is quite acceptable.

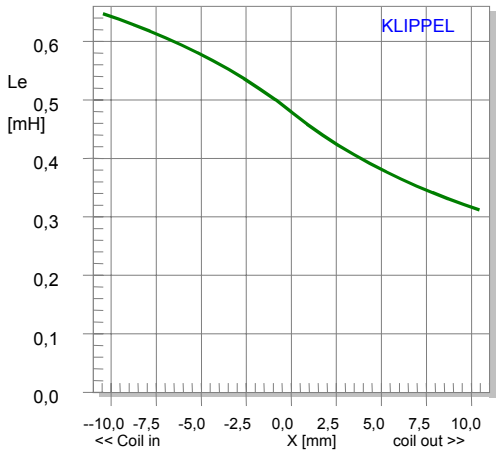

Fig. 11. Inductance versus displacement x of Driver A

The voice coil inductance $L_e(x)$ as shown in Fig. 11 has a distinct asymmetrical shape increasing when the coil is moving towards the back plate. This is typical for drivers using no short cut ring or other means for reducing the voice coil inductance.

Fundamental Component

Using the large signal parameters of the Driver A we predict the transfer responses of the driver mounted in an infinite baffle. The fundamental response in the voice coil displacement for a single excitation tone varied versus frequency and amplitude is shown in Fig. 12.

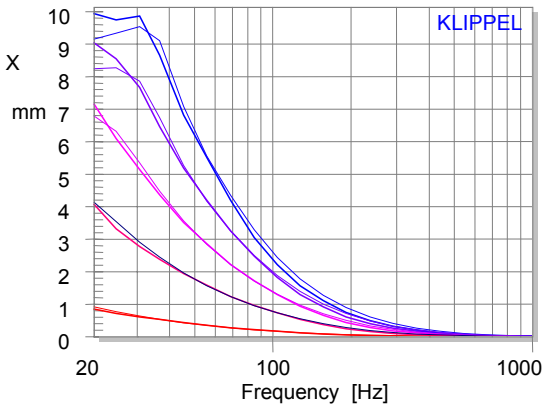

Fig. 12. Fundamental displacement x of Driver A predicted (bold lines) and measured (thin line) at peak voltage U = 1, 4.5, 8, 11.5, 15V

Five frequency sweeps are performed at different amplitudes of input voltage u(t) linearly increased from 1 to 15 V by 3.5 V steps. The predicted curves (bold lines) agree quite well with the thin curves measured by using a laser displacement meter. Both measured and predicted curves reveal an amplitude compression. Whereas the first amplitude step increases the peak displacement by 3 mm there is only an increase about 1 mm at maximal amplitude U=15 V.

DC-Component

A loudspeaker with asymmetrical parameters will rectify an AC-signal producing a DC-component in the displacement dynamically. Fig. 13 shows the predicted and measured DC-displacement versus frequency of the excitation tone at peak voltage of U=15 V.

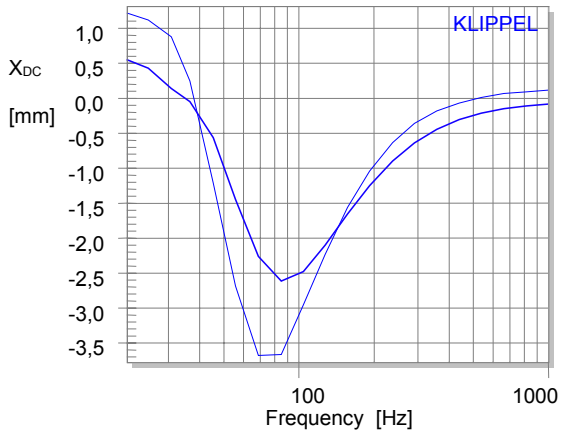

Fig. 13. Dynamically generated DC-part in voice coil displacement versus frequency of the excitation tone at U = 15 V measured (thin line) and predicted (bold line) from large signal parameters.

Both curves agree approximately indicating a positive DC displacement below the resonance frequency f_s and a substantial negative displacement above f_s. This is typical for a driver with significant $Bl(x)$-asymmetry where the phase relationship between current and displacement determines the direction of the DC-component [15]. At low frequencies $f < f_s$ the coil always moves to the Bl-maximum which is a self-adjusting feature of the motor.

At higher frequencies $f > f_s$ the coil will slide down on the slope of the *Bl(x)*-curve producing a DC-component which is in the same order of magnitude as the fundamental component as shown in Fig. 14.

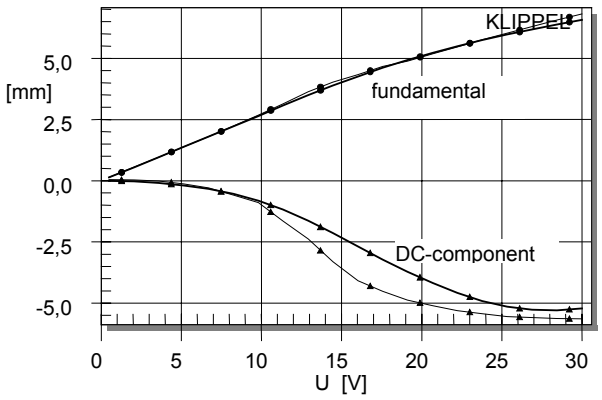

Fig. 14. Fundamental (circle) and DC-part (triangle) in voice coil displacement versus input voltage of excitation tone at f=70 Hz measured (thin line) and predicted (bold line).

This reveals an instable mechanism inherent in drivers using a voice coil in a magnetic field. Only the stiffness of suspension will produce an opposite force keeping the coil in the gap. Clearly, a suspension with higher stiffness and nonlinear characteristic will reduce the DC-displacement but also any AC-component. However, changes on the suspension will reduce the effect but does not remove the cause of the instability. This problem may be easily fixed by correcting the rest position of the coil.

Harmonic Distortion

The total harmonic distortion in the radiated sound pressure signal predicted and measured for a sinusoidal voltage signal with U_{peak} = 1 V, 8 V and 15 V are shown in Fig. 15.

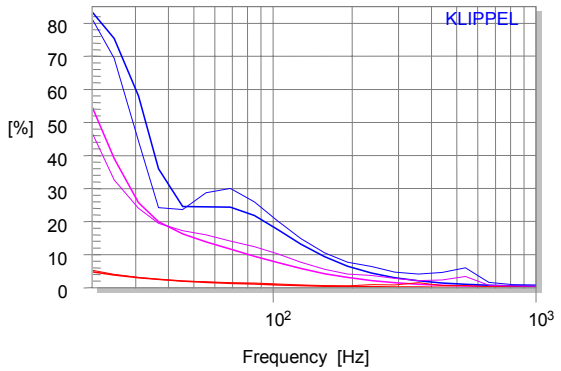

Fig. 15. Total harmonic distortion of Driver A measured (thin line) at U = 1V, 8V, 15 V and predicted (bold line) from large signal parameters

Below the resonance frequency the energy of the harmonics dominates the sound pressure output. Expressing the distortion in percent according to IEC 60268-5 we get more than 80 % for Driver A. This is a general phenomenon caused by a couple of reasons:

- the amplitude of the displacement is high for $f < fs$ producing substantial parameter variation due to $L_e(x)$, $C_{ms}(x)$ and *Bl(x)*-nonlinearities,
- the input current has a high value and is in phase with the displacement producing high motor distortion,
- fundamental component is below the cut-off frequency but the harmonic will still be radiated in the pass-band .

At higher frequencies the total distortion gradually decreases to small values. A detailed analysis of the spectral component of the second- and third order shows the relationship to the nonlinear parameters. Fig. 16 shows the measured and predicted second-order distortion as thin and bold curve, respectively. The good agreement confirms that the modeling is quite reliable and we may use the numerical tool for simulations of driver modifications. Considering only one nonlinearity while replacing all of the remaining parameters by the corresponding constant value from the rest position shows the effect of each nonlinearity separately. The asymmetry of the *Bl(x)*-nonlinearity is the dominant source of second-order distortion represented as dotted line with downward triangles because this curve is close to the measured and predicted response considering all nonlinearities. The asymmetry of the suspension causes 10 % distortion below the resonance frequency but decreases at a rate of 24 dB /octave to higher frequencies. The second-order harmonics produced by inductance $L_e(x)$ and Doppler distortion are negligible in Driver A.

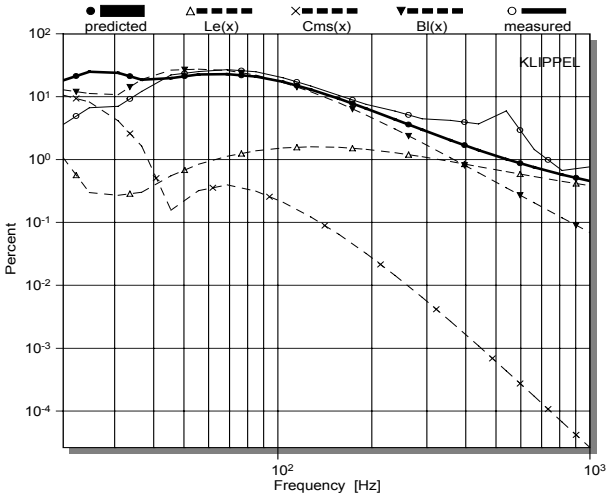

Fig. 16. Second-order harmonic distortion of Driver A measured (thin line) and predicted considering all nonlinearities (bold line) and separated nonlinearities (dashed lines)

The third-order harmonic response reveals the symmetrical variation of the nonlinear parameters primarily. However, second-order distortion caused by asymmetries will feed back to the nonlinear parameters in Fig. 3 and will be transformed into third- and higher-order distortion.

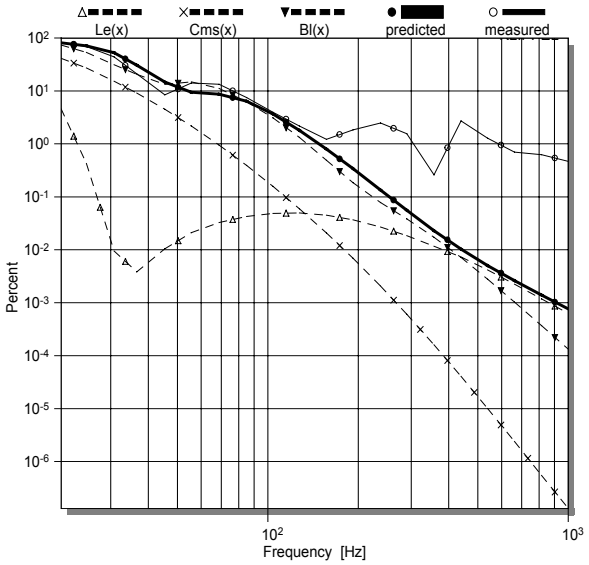

Fig. 17. Third-order harmonic distortion of Driver A measured (thin line with circle) and predicted considering all nonlinearities (bold line) and separated nonlinearities (dashed lines)

Fig. 17 shows the agreement between measured and predicted third-order distortion and a simulation of the driver modifications with separated nonlinearities. The high values of third-order distortion (80 %) is caused by the *Bl(x)* nonlinearity. The contribution of the suspension is about 6 dB lower. The inductance distortion is inaudible at values about 0.1 percent. Above 200 Hz the measured harmonic distortion is almost constant whereas the predicted distortion vanishes at a rate of about 36 dB/octave. The residual distortion of about 1 % indicates a nonlinear mechanisms which has not been considered in the current modeling.

Intermodulation Distortion

Distortion measurements using a single sinusoidal tone can not reflect intermodulation between components in the audio signal. A simple two tone signal comprising a variable tone f_1 and a second tone with constant frequency f_2 =70 Hz shows the nth-order intermodulation components at difference frequencies $f_1 - nf_2$ and summed frequencies $f_1 + nf_2$ for $n=1,2,...$ Fig. 18 shows the second-order intermodulation (n=1) in the radiated sound pressure according IEC 60268-5 for Driver A.

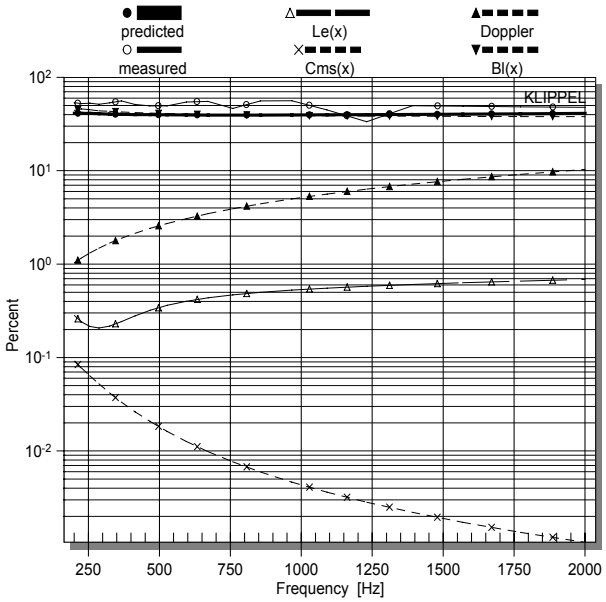

Fig. 18. Second-order intermodulation of Driver A measured (thin line) and predicted considering all nonlinearities (bold line) and separated nonlinearities (dashed lines)

Both the measurement and the prediction agree in substantial distortion which is constant at about 40%. This is typical for motor distortion caused by an asymmetry in the *Bl(x)-curve*. Intermodulation distortion of this magnitude is clear audible as a roughness of the high-frequency component.

The intermodulation due to the $L_e(x)$ nonlinearity are at a constant level of 1 % at higher frequency. The Doppler distortion increase by 6dB/octave to higher frequencies and come up to 10 % for f_1= 2kHz. The intermodulation distortion from $C_{ms}(x)$ are less than 0.1% at very low frequencies and may be neglected at higher frequencies.

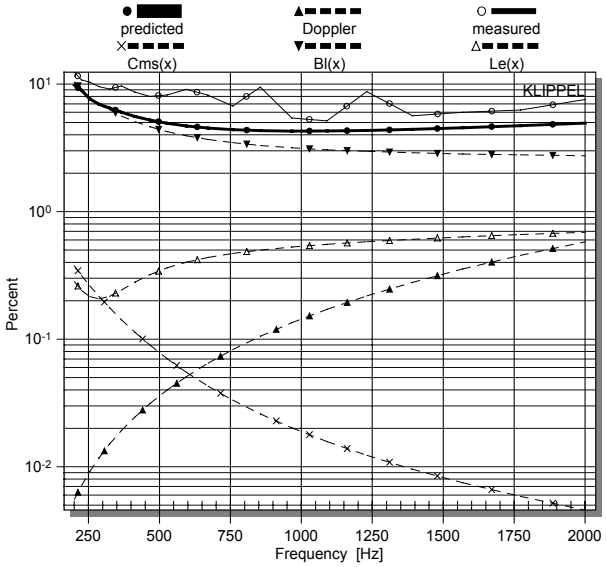

Fig. 19. Third-order intermodulation of Driver A measured (thin line) and predicted considering all nonlinearities (bold line) and separated nonlinearities (dashed lines)

The third-order intermodulation distortion (n=2) of Driver A is presented in Fig. 19. Again Bl(x) contributes most to the predicted intermodulation (5 –10 %) which are close to the values of the measurement. This is typical for drivers using a short voice coil overhang. Third-order intermodulation can not be avoided by a reasonable voice coil height maintaining sufficient efficiency of the driver. All of the other nonlinearities contribute distortion far below 1 %.

Remedy for Driver A

After performing a detailed analysis of Driver A based on parameter identification, measurement, prediction and simulation we draw conclusions for practical improvements.

Using the result of the nonlinear parameter measurement a shift of 2 mm in positive direction (coil out) is required for bringing the coil into the Bl-maximum and obtaining a symmetrical characteristic. This is a most effective action which can easily be accomplished and does not affect costs, weight and size of the driver but gives more sensitivity, more stable behavior and less distortion.

The numerical simulation shows the improvement in performance for the virtually fixed driver. Using a shifted Bl(x) curve and all of the other parameters of Driver A we calculated the second- and third-order distortion in Fig. 20.

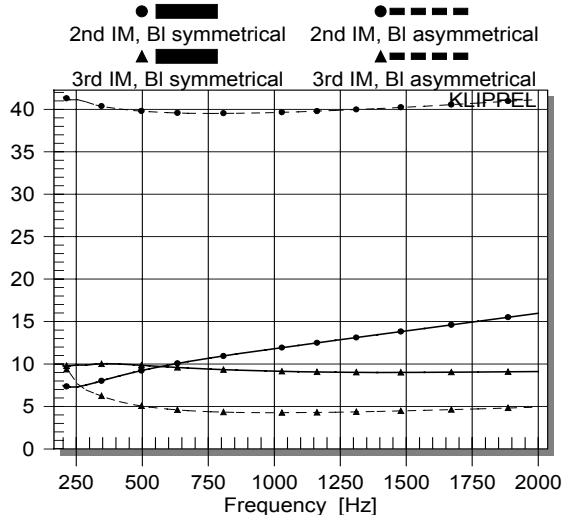

Fig. 20. Intermodulation distortion before (dotted lines) and after (bold lines) correction of the voice coil offset

The second-order distortion can be reduced by 12 dB limited now by Doppler distortion which can be easily identified by the slope going up by 6 dB/octave to higher frequencies. Operating the coil now more symmetrically the motor produces 5% more third-order distortion which is due to the short voice coil overhang. However, the third-order intermodulation is still below the Doppler distortion.

The suspension of Driver A does not need much attention because the stiffness curve is sufficiently symmetrical and the useable working range defined by suspension extends the capability of the motor defined by the coil height.

A short cut ring is not required because the Doppler distortion is almost 20 dB higher than the intermodulation caused by the inductance nonlinearity $L_e(x)$.

Driver B

The second example in the case study is a five inch woofer with a significant voice coil overhang optimally adjusted in a symmetrical magnetic field as shown in Fig. 21.

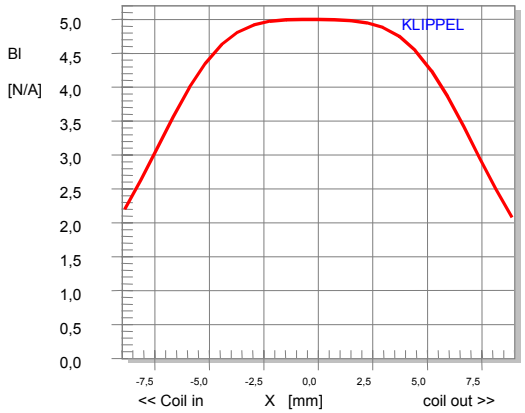

Fig. 21. Force factor characteristic $Bl(x)$ versus displacement x of Driver B

For small displacement the Bl-characteristic is almost constant causing low amount of motor distortion but for higher displacement where the overhang is exhausted the $Bl(x)$ decreases at a steep slope. However, not the voice coil overhang but the voice coil height determines the maximal displacement X_{max}= 8 mm defined here by the displacement where the instantaneous Bl-product is at half the value at the rest position $Bl(x=0)$. Thus driving this speaker to the limits of the motor we get similar third-order distortion as in an equal-length configuration.

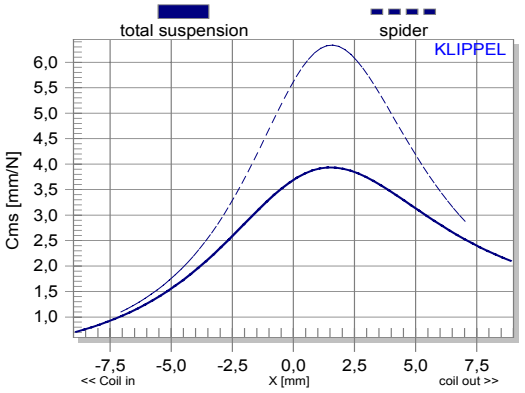

Fig. 22. Compliance $C_{ms}(x)$ versus displacement x for the total suspension of Driver B (bold line) and for the separated spider (dotted line)

In contrast to the almost ideal symmetry of the Bl-characteristic the bold curve in Fig. 22 reveals a nonlinear $C_{ms}(x)$ characteristic with a distinct asymmetry. For positive displacement the compliance is more than 4 times softer than for the same negative displacement. This effect is not restricted to a particular unit but found on all drivers using the same suspension components. To localize the cause of this asymmetry 95 % of the surround material has been cut away down to small stripes ensuring sufficient guidance of the moving assembly. The result of a second compliance measurement is presented in Fig. 22 as a thin line which can be assigned to the spider that clearly dominates now the remaining suspension. Despite a loss of stiffness both curves show the same asymmetrical characteristic indicating the spider as the cause of the problem.

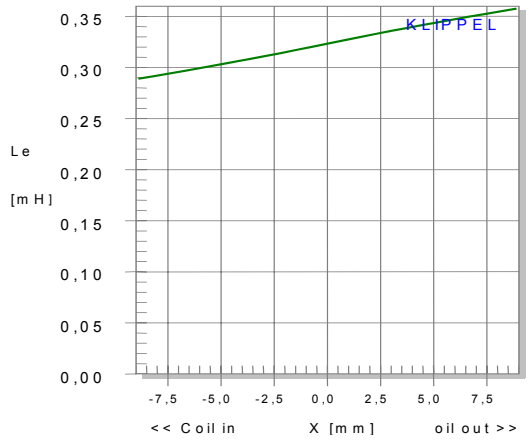

Fig. 23. Inductance versus displacement of Driver B

The inductance $L_e(x)$ presented in Fig. 23 increases with positive voice coil displacement (coil out). This is an atypical behavior indicating that a short cut ring or copper cap is used and is located below the pole plate.

Fundamental Component

The fundamental response predicted at equidistant voltage steps reveals in Fig. 24 the typical amplitude compression at X_{max}= 8 mm which is quite obvious for frequencies below and above the resonance frequency.

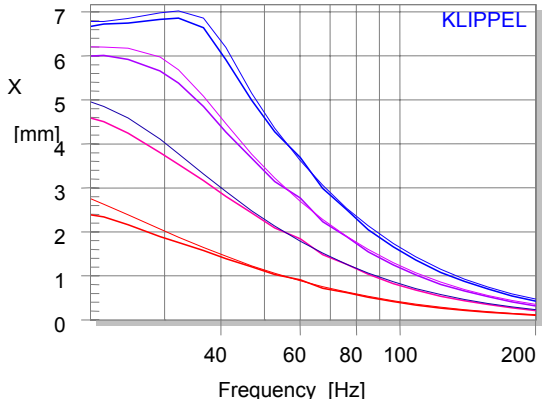

Fig. 24. Fundamental displacement x of Driver A predicted (bold lines) and measured (thin line) at peak voltage U = 2, 4, 6, 8 V.

DC-Component

Driver B also produces a significant DC-component as predicted and measured in Fig. 25.

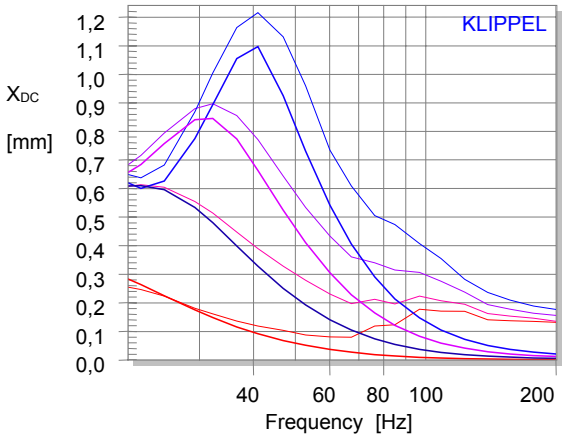

Fig. 25. Dynamically generated DC-part in voice coil displacement of Driver B versus frequency of the excitation tone at U = 2, 4, 6, 8 V measured (thin line) and predicted (bold line) from large signal parameters.

In contrast to Driver A the DC component is always directed in positive direction and the DC component is maximal at the resonance frequency for an input voltage of U = 8 V. At this frequency $f=f_s$ only the compliance can produce a DC component of significant value that moves the coil always towards a region of lower stiffness. At frequencies far below the resonance f=20 Hz the DC-component rises rapidly by increasing U= 2 to 4 V, stagnates at the same value X_{DC}= 0.7 mm for U= 6 V and even decreases for higher values U=8V. This is caused by the symmetrical $Bl(x)$ nonlinearity which becomes active for higher displacement and produces a DC-component which always pushes the coil back to the Bl-maximum for $f < f_s$.

At higher frequencies f > 100 Hz all of the measured curves are shifted by 0.2 mm to the positive direction for all input amplitudes. This is due to the memory of the suspension. The measurement has been performed with a frequency sweep starting at 20 Hz up to higher frequencies. The suspension get accustomed to the permanent DC-component generated at low frequencies and the suspension forgets its original rest position (hysteresis) or slowly approaches to the old position (creep).

The generation of a DC-component is a critical indication about the stability of the driver. The value of the DC-component is usually much higher than the amplitude of any harmonic or intermodulation in the displacement for a couple of reasons:

- all AC-components rectified by an asymmetrical nonlinearity will contribute to the DC-component,
- the $Bl(x)$ nonlinearity causes instability above the resonance $f > f_s$,
- the DC-component generated in a driver finds usually a higher compliance of the suspension than other AC components at higher frequencies due to suspension creep,
- the DC-component generated by a driver mounted in a "sealed" enclosure is not reduced by the stiffness of the enclosed air since a small leakage is always present and required,
- turbulences and asymmetries in the port and other acoustical parts may rectify the air flow, changing the static pressures and generating a DC-displacement.

Harmonic Distortion

Fig. 26 shows a good agreement between the measured and predicted total harmonic distortion for four frequency sweeps at equidistant amplitude levels.

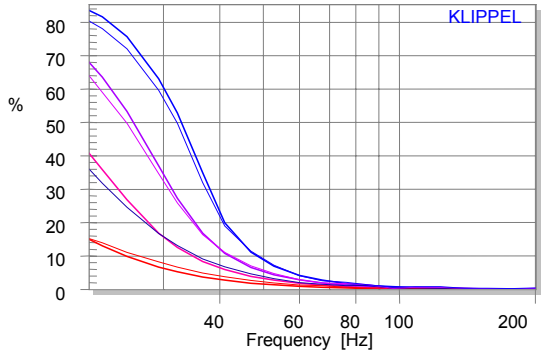

Fig. 26. Total harmonic distortion of Driver B measured (thin line) at U = 2, 4, 6, 8V and predicted (bold line) from large signal parameters

The second-order harmonic distortion presented in Fig. 27 show the effect of the parameter asymmetries. Over a wide frequency range the measured and predicted responses are in good agreement.

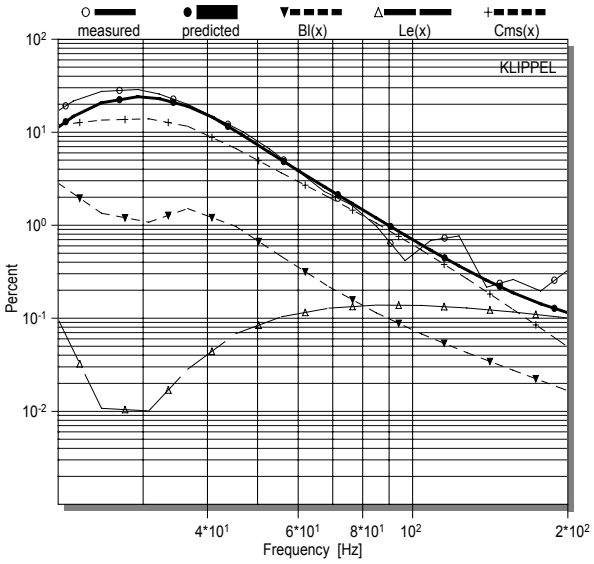

Fig. 27. Second-order harmonic distortion of Driver B measured (thin line) and predicted considering all nonlinearities (bold line) and separated nonlinearities (dashed lines)

The simulation of a modified driver which has only the nonlinear suspension represented by $C_{ms}(x)$ will produce almost the same amount of distortion. The contribution from the $Bl(x)$-nonlinearity is about 20 dB lower. Both kinds of distortion decrease by a rate of about 24 dB/octave to higher frequencies. Only the distortion from $L_e(x)$ nonlinearity remains nearly constant at higher frequencies and becomes dominant above 200 Hz. However, the short cut ring used in Driver B keeps the inductance distortion at a very low level (about 0.1 %).

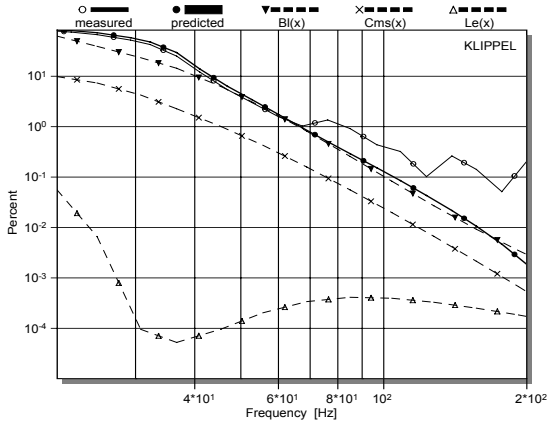

Fig. 28. Third-order harmonic distortion of Driver B measured (thin line) and predicted considering all nonlinearities (bold line) and separated nonlinearities (dashed lines)

The third-order harmonic is the dominant component of the total harmonic distortion for an input voltage of U= 8V. For high distortion values at low frequencies the prediction agrees almost perfectly with the direct measurement. Above 100 Hz where the distortion is far below 1 % we see the effect of other nonlinear mechanisms not considered in the current modeling. The simulation reveals that the symmetrical decay of the Bl-product at higher amplitudes is the dominant cause of the third-order distortion. The stiffness distortion are about 20 dB lower and the contribution from the inductance is negligible.

Intermodulation Distortion

The intermodulation distortion between two tones reveals properties of Driver B which can not be assessed by measuring harmonic distortion. The first tone with variable frequency f_1 and voltage U_1=4 V_{peak} stands for a voice component in the pass-band. A second tone at f_2=20 Hz with input voltage U_2= 8 V_{peak} generates a large voice coil displacement of about 7 mm peak and represents a bass component.

The measured and predicted second-order intermodulation presented in Fig. 29 versus frequency f_1 are in good agreement.

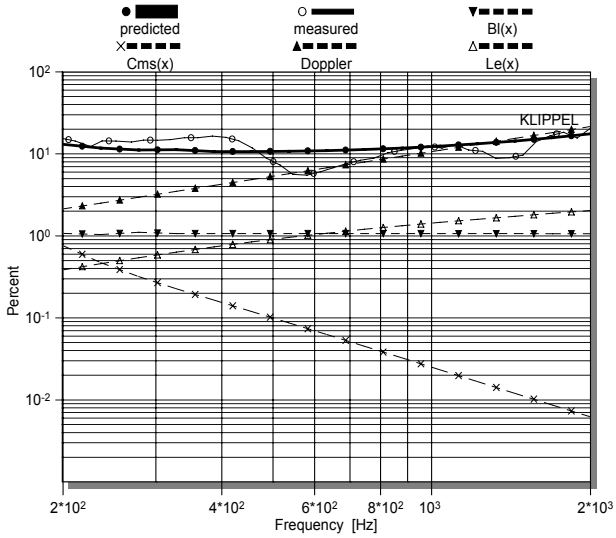

Fig. 29. Second-order intermodulation of Driver B measured (thin line) and predicted considering all nonlinearities (bold line) and separated nonlinearities (dashed lines)

Both curves rise gradually from about 10% at f_l=200 Hz to almost 20% at f_l=2 kHz. The predicted response shows less fluctuations than the measured curve because the simple lumped parameter model can not reflect the mechanical and acoustical modes at higher frequencies. However, this is a linear phenomenon which may be considered in the modeling by connecting a linear system with the measured linear transfer response after the nonlinear model.

The simulation of the driver with separated nonlinearities shows that the Doppler effect is the most dominant source of distortion at higher frequencies. Surprisingly, at low frequencies f_l=200 Hz all of the isolated nonlinearities produce distortion which is about 20 dB below the measured and predicted curve.

For example *Bl(x)*-nonlinearity considered separately produces intermodulation distortion of about 1 % only. This corresponds with the very symmetrical Bl(x)-characteristic due to the symmetrical geometry of the magnetic field in the gap and the optimal rest position of the coil. The $C_{MS}(x)$ characteristic considered alone is not capable in producing significant intermodulation. Summing up the effect of the separated nonlinearities will not result in the predicted response considering all nonlinear parameters simultaneously. Only an interaction between asymmetrical $C_{MS}(x)$ and nonlinear *Bl(x)*-characteristic explains the high second-order intermodulation in Driver B.

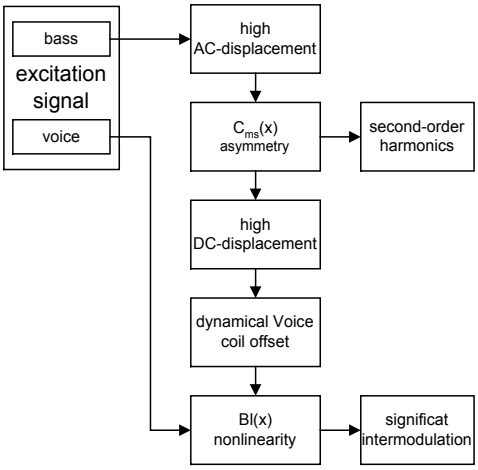

Fig. 30. Interaction between suspension and motor nonlinearity

The complicated interplay between the two nonlinearities is illustrated in Fig. 30. The second tone at f_2=20 Hz represents a bass component in the audio signal producing high AC-displacement of the coil. The asymmetry of the suspension rectifies the AC-signal and generates a high DC-component in the displacement. This mechanism so far produces some second-order harmonics of f_2 but do not distort the first f_1 at higher frequencies directly. However, the generated DC-displacement will push the coil dynamically about 1 mm in positive direction and will deteriorate the symmetrical working point in the *Bl(x)*-characteristic. Finally, the steep right slope of the *Bl(x)*-curve starting at x = 7 mm will produce significant second-order intermodulation of the tone f_1.

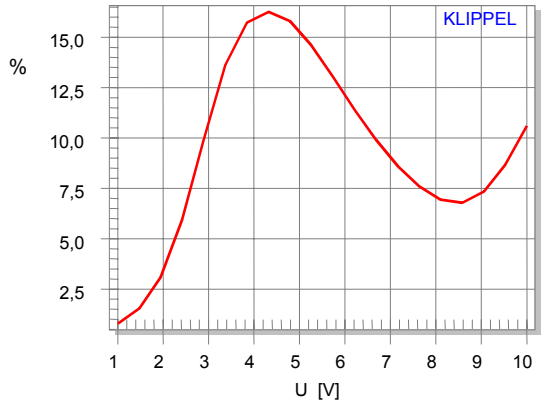

Fig. 31. Amplitude of second-order distortion versus input voltage U of the two-tone signal f_2= 30 Hz and f_1=200 Hz.

Distortion measurements performed at a single amplitude can not reflect the complicated amplitude characteristic an may lead to wrong conclusions. For example, Fig. 31 shows the amplitude of the second-order intermodulation versus input voltage U, increasing rapidly below 4 V, stagnating and decreasing to half the value at 9 V. In other cases where the motor becomes instable (for example Driver A, for $f > f_s$) the distortion may grow faster with rising input amplitude. Performing sweeps both versus amplitude and frequency are required for interpreting distortion values correctly.

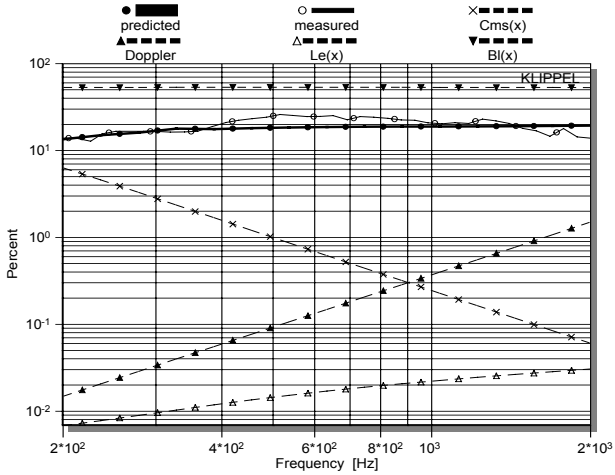

Fig. 32. Third-order Intermodulation of Driver B measured (thin line) and predicted considering all nonlinearities (bold line) and simulated driver modifications considering separated nonlinearities only (dashed lines)

The measured third-order intermodulation distortion is at a almost constant value (20%) independent from the frequencies f_1 and agrees with the predicted curve considering all nonlinearities of Driver B as shown in Fig. 32. Switching off all driver nonlinearities but considering *Bl(x)*–nonlinearity only we get a much higher value of 50% because driver B with a linear suspension $C_{MS}(x)=C_{MS}(0)=const.$ will produce a much higher displacement resulting in higher motor distortion. Clearly, *Bl(x)*–nonlinearity is the dominant source of third-order intermodulation.

Remedy for Driver B

The performance of the driver may be improved by reducing the asymmetry of the $C_{ms}(x)$-characteristic. The spider, identified as

the critical component has to be replaced or optimized by try-and error-methods or FEM-modeling. This process requires some time in development but will not increase the cost and weight of the final product.
The benefit of using a new spider may be evaluated by simulation the second-order intermodulation with symmetrical characteristic (bold lines) in Fig. 33 contrasted with the results of the original characteristic (dashed line).

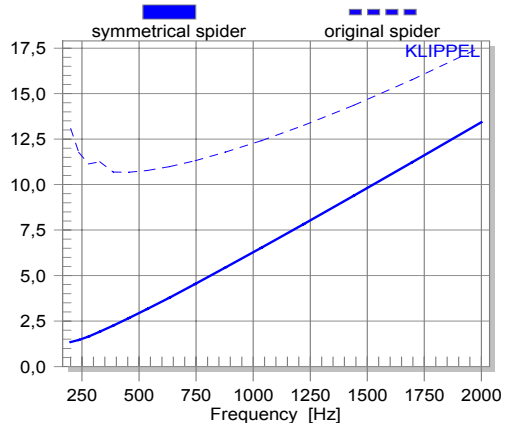

Fig. 33. Second-order intermodulation distortion versus frequency for input voltages U= 4 Volt with original and symmetrical spider.

We will achieve up to 20 dB reduction of the second-order intermodulation at low and middle frequencies only restricted by the remaining Doppler distortion which is directly related to the frequency f_1 and maximal voice coil displacement x. The Doppler distortion may be accepted as a physical limit determined by the size of the diaphragm, the upper cut-off frequency of the driver and the expected sound pressure at low frequencies.
The motor with the symmetrical *Bl(x)* characteristic does not need not much attention. Only if the sensitivity of the driver is an issue we have to evaluate the benefit of the relatively long coil overhang for the distortion reduction at small and medium amplitudes. The driver operated at maximal displacement X_{max}= 8 mm produces almost the same amount of distortion as an equal-length configuration but is usually less efficient.
The short cut ring fulfills its task in keeping the inductance distortion below 1 – 2 %. Shifting the ring in positive direction, reducing the height of the ring or replacing the ring by a copper cap removes the overcompensation for negative displacements giving even less inductance distortion without increasing the cost of the driver.

Conclusion

The good agreement between measured and predicted transfer responses shows that the current state of loudspeaker modeling, parameter identification and numerical calculation can describe the large signal behavior of real loudspeaker accurately. It seems sufficient to consider only the dominant nonlinearities in the modeling. The lumped parameter model with thermal and nonlinear parameters is a simple and useful basis for design, assessment and diagnostics of woofer, mid-range drivers, headphones, shakers and other electro-dynamical transducers mounted in different kinds of enclosure (band-pass, vented, sealed). Only a few number of large signal parameters evolved from traditional linear modeling are required and may be measured by system identification techniques. The set of nonlinear equations may be solved numerically for any excitation signal in real time on a personal computer and provides all of the state variables (sound pressure, displacement, current, volume velocity, temperature, ...) which may be subjected to a spectral analysis. Thus the prediction is an interesting, convenient alternative to direct measurement because it dispenses with special sensors for monitoring mechanical and acoustical signals in the speaker. Furthermore, a unique prototype may be assessed non-destructively at the limits and above.
The simulation applies the same tools to "virtual" speakers before the first prototype has been finished, to study the large signal behavior in detail or to investigate a variety of design choices. There are plenty of new possibilities only a few examples are given in this paper.
Both measurement, prediction and simulation techniques requires a simple but critical excitation signal. A two-tone signal varied in frequency and amplitude reveals the most important information about fundamental, DC-components, harmonics and intermodulation. The measurement of the harmonic distortion is sufficient to assess the suspension distortion caused by the $C_{ms}(x)$-nonlinearity which are bounded to low frequencies. Force factor Bl(x) and other nonlinearities of the motor and the radiation produce significant summed- and difference intermodulation between a low- and high-frequency component. Using a second tone at the resonance frequency $f_2=f_s$ and measuring the modulation distortion according IEC 60268-5 versus frequency f_1 is a necessary supplement of the measurement of harmonics. Sufficient variation of the input amplitude of the two-tone signal is required to consider the complicated relationship between input and output amplitude (compression and expansion effects).
The most informative variables of the speaker is the radiated sound pressure signal and the voice coil displacement. Normally the harmonic and intermodulation distortion are only evaluated in the sound pressure output. The fundamental displacement is crucial for defining the maximal displacement X_{max}. The measurement or prediction of the DC-displacement is a critical test on the stability of the driver and loudspeaker system because it couples all the different nonlinear mechanisms causing complicated interactions. Driver B presented in this paper is an example for a high-quality motor that produces modulation distortion initiated by a suspension problem.
The simulation technique clearly shows the effect of each separated nonlinearity, the dominant source of distortion and the physical cause limiting the speaker's output.
This information become available in an early phase of driver and system development, speeding up the investigation of design choices, substituting time consuming measurements and enabling the engineer to optimize speakers in the large signal domain.

References

[1] R. H. Small, „Direct-Radiator Loudspeaker System Analysis," J. Audio Eng. Soc., vol. 20, pp. 383 – 395 (1972 June).

[2] R.H. Small, „Closed-Box Loudspeaker Systems, Part I: Analysis," J. Audio Eng. Soc., vol. 20, pp. 798 – 808 (1972 Dec.).

[3] A. N. Thiele, „Loudspeakers in Vented Boxes: Part I and II," in Loudspeakers, vol. 1 (Audio Eng. Society, New York, 1978).

[4] D. Button, "A Loudspeaker Motor Structure for Very High Power Handling and High Linear Excursion," J. Audio Eng. Soc., vol. 36, pp. 788 – 796, (October 1988).

[5] C. A. Henricksen, "Heat-Transfer Mechanisms in Loudspeakers: Analysis, Measurement, and Design," J. Audio Eng. Soc., vol. 35, pp. 778 – 791, (October 1987).

[6] E. R. Olsen and K.B. Christensen, "Nonlinear Modeling of Low Frequency Loudspeakers - a more complete model," presented at the 100th convention Audio Eng. Soc., Copenhagen, May 11-14, 1996, preprint 4205.

[7] M.H. Knudsen and J.G. Jensen, "Low-Frequency Loudspeaker Models that Include Suspension Creep," *J. Audio Eng. Soc.,* vol. 41, pp. 3 - 18, (Jan./Feb. 1993).

[8] A. Dobrucki, "Nontypical Effects in an Electrodynamic Loudspeaker with a Nonhomogeneous Magnetic Field in the Air Gap and Nonlinear Suspension," *J. Audio Eng. Soc.,* vol. 42, pp. 565 - 576, (July./Aug. 1994).

[9] A. J. M. Kaizer, "Modeling of the Nonlinear Response of an Electrodynamic Loudspeaker by a Volterra Series Expansion," *J. Audio Eng. Soc*., vol. 35, pp. 421-433 (1987 June).

[10] W. Klippel, "Nonlinear Large-Signal Behavior of Electrodynamic Loudspeakers at Low Frequencies," *J. Audio Eng. Soc*. , vol. 40, pp. 483-496 (1992).

[11] J.W. Noris, "Nonlinear Dynamical Behavior of a Moving Voice Coil," presented at the 105th Convention of the Audio Engineering Society, San Francisco, September 26-29, 1998, preprint 4785.

[12] D. Clark, „Precision Measurement of Loudspeaker Parameters," *J. Audio Eng. Soc.* vol. 45, pp. 129 - 140 (1997 March).

[13] W. Klippel, "Measurement of Large-Signal Parameters of Electrodynamic Transducer," presented at the 107th Convention of the Audio Engineering Society, New York, September 24-27, 1999, preprint 5008.

[14] W. Klippel, "Distortion Analyzer – a New Tool for Assessing and Improving Electrodynamic Transducer," presented at the 108th Convention of the Audio Engineering Society, Paris, February 19-22, 2000, preprint 5109.

[15] W. Klippel, "Diagnosis and Remedy of Nonlinearities in Electro-dynamical Woofers ," presented at the 109th Convention of the Audio Engineering Society, Los Angeles, September 22-25, 2000, preprint 5261